Relaxation Paths from a Conical Intersection: The Mechanism of Product Formation in the Cyclohexadiene/Hexatriene Photochemical Interconversion

Marco Garavelli,[†] Paolo Celani,[‡] Monica Fato,[†] Michael J. Bearpark,[‡] Barry R. Smith,[‡] Massimo Olivucci,*[,†] and Michael A. Robb*[,‡]

Dipartimento di Chimica "G. Ciamician" dell'Università di Bologna, Via Selmi 2, 40126 Bologna, Italy, and Department of Chemistry, King's College, London, Strand, London WC2R 2LS, U.K.

Received: May 29, 1996; In Final Form: October 30, 1996[⊗]

An algorithm for the computation of initial relaxation directions (IRD) from the tip of a conical intersection is discussed. The steepest descent paths that can be computed starting from these IRD provide a description of the ground state relaxation of the "cold" excited state species that occur in organic photochemistry where slow motion and/or thermal equilibration is possible (such as in cool jet, in matrices, and in solution). Under such conditions we show that the central conclusions drawn from a search for IRD and those obtained from semiclassical trajectory computations are the same. In this paper, IRD computations are used to investigate the mechanism of photoproduct formation and distribution in the photolysis of cyclohexadiene (CHD) and *cZc*-hexatriene (*cZc*-HT). A systematic search for the IRD in the region of the $2A_1/1A_1$ conical intersection (see Celani, P.; Ottani, S.; Olivucci, M.; Bernardi, F.; Robb, M. A. *J. Am. Chem. Soc.* 1994, *116*, 10141−10151) located on the $2A_1$ potential energy surface of these systems yields three relaxation paths. The first two paths, which start in the strict vicinity of the intersection, are nearly equivalent energetically and lead to production of CHD and *cZc*-HT, respectively. The third path, which begins at a much larger distance, lies higher in energy and ends at a methylenecyclopentene diradical (MCPD) minimum. Further, while the first two paths define directions that form a 60° angle with the excited state entry channel (i.e. the direction along where the conical intersection region is entered), the third path is orthogonal. It is shown that these findings are consistent with the experimental observations which show nearly equivalent quantum yields for CHD and *cZc*-HT and no production of MCPD. The results of the IRD computations have been validated by investigating the decay dynamics of trajectories starting from a "circle" of points around the conical intersection, with the initial kinetic energy distributed in randomly sampled vibrational modes. These computations have been carried out using a trajectory-surface-hopping (TSH) method and a hybrid molecular mechanics valence bond (MM−VB) force field to model the ab initio potentials.

1. Introduction

Recent studies (see for example the "highlight" article by M. Klessinger[1]) have demonstrated that conical intersections[2] provide a common channel for the radiationless deactivation of photoexcited organic molecules to a lower state of the same spin multiplicity. In many cases this deactivation results in a photochemical reaction,[3] and thus the decay at a conical intersection initiates the process of photoproduct formation. In this paper, we use a new computational technique to investigate the *structure* of the potential energy surface which connects (adiabatically) an excited state intermediate to the ground state product valleys through a conical intersection point. We will show that such *structural* information may be used to gain insight into the mechanism of photoproduct formation from "cold" excited state reactants.

Advances in laser technology and new spectroscopic techniques allow one to carry out photochemical reactions in a relatively cold environment where the excited state reactant has a small/controlled amount of vibrational excess energy. For instance, with lasers it is possible to gradually increase the excited state "temperature" above the 0−0 transition to a point where a radiationless decay channel opens up and a photochemical transformation occurs. This has been recently observed in jet-cooled polyenes[4] where we have shown that the decay channel corresponds to a conical intersection located just after a $2A_1$ transition state.[5] Due to the small excited state momentum, the decay of these systems must take place right in the *vicinity* of the conical intersection where the energy gap is small (i.e. ∼1 kcal mol^{-1}).[6] Another environment where the excited state reactant has a small amount of vibrational energy is the condensed phase (including cold matrices). In fact, it has been recently shown, both computationally[7] and experimentally,[8] that energy transfer to the solvent molecules and therefore vibrational cooling and energy redistribution of an initially hot solute are already active on the subpicosecond time scale. An excited state lifetime greater than a few picoseconds has been observed for the photochemical ring opening of cyclohexa-1,3-diene (CHD) at room temperature in cyclohexane solution.[9] Thus, in this case, the excess vibrational energy accumulated after relaxation from the Franck Condon (FC) region is, at least in part, lost to surroundings and subsequent radiationless decay occurs in conditions approaching thermal equilibrium.

Decay through a conical intersection and the subsequent evolution on the ground state surface can be studied using quantum or semiclassical dynamics.[10] For a cold or thermalized excited state of a sizeable organic molecule, the structure of the potential energy surface is expected to play the dominant role in determining the *initial* molecular motion in the decay region. Thus, one expects that excited state stationary points and minimum energy paths (MEP)[11] will provide the important mechanistic information. For a photochemical reaction involv-

[†] Università di Bologna.
[‡] King's College.
[⊗] Abstract published in *Advance ACS Abstracts,* January 1, 1997.

S1089-5639(96)01554-X CCC: $14.00

SCHEME 1

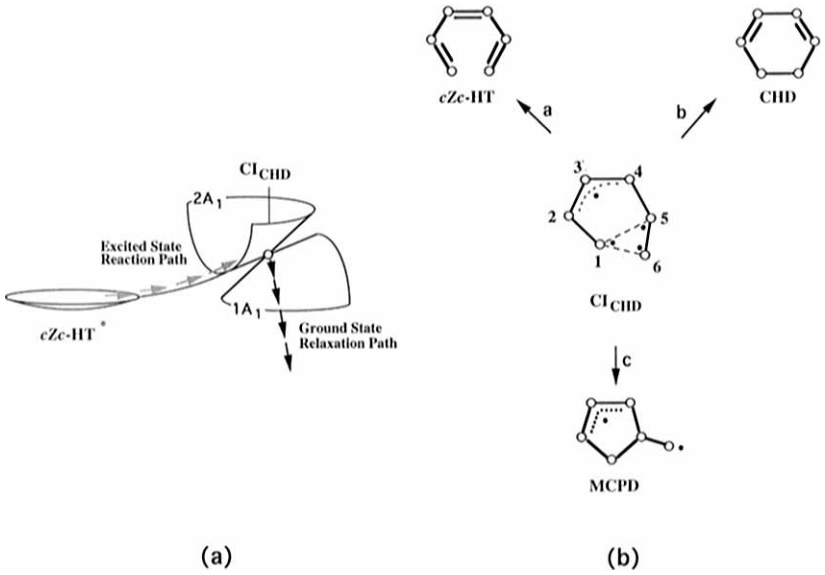

ing decay at a conical intersection, the MEP coordinate will have two branches. The first (excited state) branch describes the evolution of the molecular structure of the excited state intermediate until a decay point is accessed. At this point, the second (ground state) branch of the reaction coordinate begins, which describes the relaxation process ultimately leading to product formation. The excited state MEP and low-lying conical intersections which describe the excited state reaction coordinate have presently been characterized for several systems.[3] However, the characterization of the associated ground state coordinate, which describes the relaxation occurring after the decay, appears to be an outstanding problem. Indeed, while the location of minima, transition states, conical intersections, and MEP on the excited state potential energy surface can be accomplished with existing methods,[12] the problem of determining ground state relaxation paths, starting in the vicinity of a conical intersection, does not seem to have been considered before. We shall see below that the ground state relaxation paths departing from a single conical intersection point can be unambiguously defined and computed with a gradient-driven algorithm. Under conditions of low vibrational excess energy, we also demonstrate that the semiclassical dynamics yields the same mechanistic information.

We have recently reported a theoretical study of the first singlet excited state ($2A_1$) of *cZc*-hexa-1,3,5-triene (*cZc*-HT) and CHD.[13] These molecules are important active centers of many photochromic materials[14] and can be photochemically interconverted via direct irradiation experiments.[15] Irradiation at 254 nm transforms 2,5-di-*tert*-butylhexa-1,3,5-triene (a hexatriene with a dominant *cZc* equilibrium conformation) into the corresponding CHD with a 0.54 quantum yield. The reverse reaction transforms 1,4-di-*tert*-butylcyclohexa-1,3-diene into the corresponding HT with a 0.46 quantum yield.[16] Consistently, the computed structure of the low-lying part of the $2A_1$ potential energy surface of these molecules shows that both the direct (CHD → *cZc*-HT) and reverse (*cZc*-HT → CHD) photochemical reactions involve the formation and decay of a common excited state intermediate (see Scheme 1a). This intermediate corresponds to excited state *cZc*-HT (*cZc*-HT*), and it is predicted to decay to the ground ($1A_1$) state via a conical intersection (CI_{CHD}) which has been located ∼1 kcal mol^{-1} above *cZc*-HT* (see point (i) in the Supporting Information for a detailed discussion of the $2A_1 \rightarrow 1A_1$ decay). Relaxation from CI_{CHD} may occur, in principle, along three different routes as illustrated in Scheme 1b. Each route is associated with a different bond formation mode which is, in turn, driven by the recoupling of four weakly interacting electrons (Scheme 1b). Accordingly, route a leads to relaxation toward *cZc*-HT, route b leads to CHD, and route c leads to a methylenecyclopentene diradical (MCPD).

In the present paper we investigate the mechanism of product formation in CHD photochemistry in the limit of a cold excited state. This will be accomplished via a systematic search for the ground state relaxation paths departing in the region of CI_{CHD} and defining the "accessible" product valleys. In other words, since it is experimentally established that, in solution, the CHD $2A_1$ state has a picosecond lifetime,[9] we assume that (i) *the photoproducts originate from an excited state intermediate which is sufficiently cold that the ground state trajectories lie very close to the computed MEP* and (ii) *the surface hop occurs in the vicinity of the optimized conical intersection point.* The validity of these assumptions is investigated in section 4 via semiclassical dynamics calculations using a 36-dimensional, hybrid quantum-mechanical/force-field potential (MM−VB) which reproduces the structure of the CHD ab initio energy surface.

2. Initial Relaxation Directions from a Conical Intersection

The topography of the potential energy surfaces in the vicinity of a conical intersection has been analyzed by Ruedenberg et al.,[17] and in this paper we will use their terminology. In general, at a point of conical intersection one can identify two characteristic types of molecular structure deformation. The first type causes the excited and ground state energies to remain degenerate and defines the "intersection space". This space is $n - 2$ dimensional in the sense that there are $n - 2$ independent directions ($\mathbf{x}_3$, $\mathbf{x}_4$, ..., $\mathbf{x}_n$) of nuclear motion which will preserve the degeneracy (n indicates the number of vibrational degrees of freedom of the molecule under investigation). The second type of deformation lifts the degeneracy and defines the "branching space" which comprises the remaining two independent directions of nuclear motion ($\mathbf{x}_1$ and $\mathbf{x}_2$). Any molecular motion which has a non-zero component along at least one of these directions ($\mathbf{x}_1$ and $\mathbf{x}_2$) lifts the degeneracy and takes the system away from the conical intersection. As illustrated in Figure 1a, the conical intersection vertex forms a "singularity" on each adiabatic potential energy surface ($\mathbf{E}_{ex}$ and $\mathbf{E}_{gs}$), since

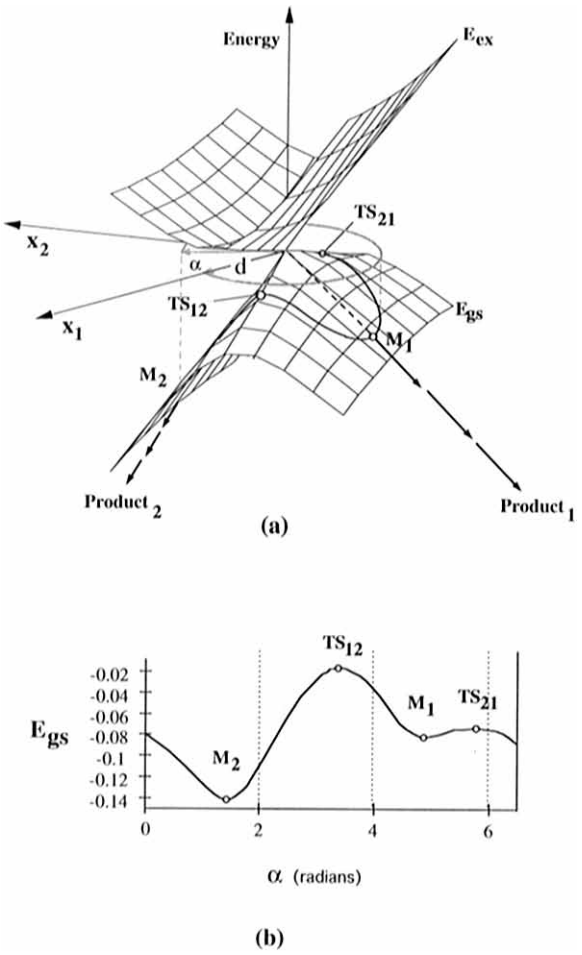

Figure 1. (a) Three-dimensional view of the shape of model excited ($\mathbf{E}_{ex}$) and ground ($\mathbf{E}_{gs}$) state potential energy surfaces near a conical intersection point for the general case of an elliptic cone and tilted axes ($\mathbf{E}_{gs/ex} = a\mathbf{x}_1 + b\mathbf{x}_2 \pm (\mathbf{x}_1^2 + c\mathbf{x}_2^2)^{1/2}$ with $a = 0.3$, $b = 0.3$ and $c = 0.4$).[17] The circle on the coordinate plane (x_1,x_2) indicates the position of a circular cross section defined by $d = 0.1$ and $0.0 < \alpha < 2\pi$. (b) $\mathbf{E}_{gs}$ energy profile along the circle defined in Figure 1a. The points M_1 and M_2 correspond to the two energy minima located along the circular cross section. The points TS_{12} and TS_{21} correspond to the two transition structures connecting M_1 and M_2.

SCHEME 2

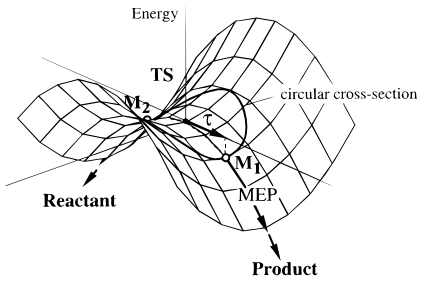

its slope and curvature along $\mathbf{x}_1$ and $\mathbf{x}_2$ are not smooth functions of the molecular deformation.

The MEP connecting the reactant to the product of a thermal reaction is uniquely defined by the associated transition structure (TS). The direction of the transition vector (i.e. the normal coordinate corresponding to the imaginary frequency of the TS) is used to start a MEP computation. One takes a small step along this vector (shown as $\boldsymbol{\tau}$ in Scheme 2) to points M_1 or M_2 and then follows the steepest descent paths connecting this point to the product or reactant well. The small step vector $\boldsymbol{\tau}$ defines the *initial relaxation direction* (IRD) toward the product (taking the positive direction of $\boldsymbol{\tau}$) or reactant (taking the negative direction of $\boldsymbol{\tau}$). This procedure cannot be used to find the IRD for a photochemical reaction since, as discussed above, a conical intersection is a singularity and there is no such unique direction $\boldsymbol{\tau}$ for this first step (i.e. a frequency computation cannot be performed at a conical intersection point).

However, one can devise a simple procedure for defining the IRD at a TS that does not use the transition vector $\boldsymbol{\tau}$. If one computes the energy of the system along a circular cross section centered at the TS as illustrated in Scheme 2, then provided the radius of the circle is small enough, the energy minima M_1 and M_2 located on the circular cross section provide an alternative but equivalent definition of the direction of relaxation toward the product and reactant. While one would not advocate such a procedure as a practical approach, such a method would, in fact, yield a correct IRD in the absence of a transition vector. We now proceed to show how the IRD can be defined in an analogous manner for a conical intersection.

In Figure 1a we show the potential energy surface for a "model" elliptic conical intersection[17] plotted along the branching plane (x_1,x_2). Because the cone is elliptic (i.e. the base of the cone is an ellipse rather than a circle), there are two "steep" sides of the ground state cone surface and two "ridges". It is thus obvious that there are two preferential directions of downhill motion located on the steep sides of the ground state cone surface. Analogous to the case of a transition structure, a simple procedure for defining these directions involves the computation of the energy profile along a circular cross section of the branching plane centered on the vertex of the cone (0,0) as illustrated in Figure 1a. This energy profile is given in Figure 1b as a function of the angle α and for a suitable choice of the radius *d*. It can be seen that the profile contains two different energy minima. These minima (M_1 and M_2 in Figure 1) uniquely define the IRD from the vertex of the cone. The two steepest descent lines starting at M_1 and M_2 uniquely define two MEP describing the relaxation processes. Notice that there are also two energy maxima TS_{21} and TS_{12} in Figure 1b. These can be interpreted as the "transition structures" connecting M_1 and M_2 along the chosen circular cross section. It can be seen in Figure 1a that these transition structures locate the energy ridges which separate the IRD "valleys" located by M_1 and M_2. Thus, while there is no analogue of the transition vector for a conical intersection, the simple case of an elliptic cone shows that the IRD are still uniquely defined in terms of M_1 and M_2. *Notice that while the IRD from a TS connect the reactant to the product, the IRD from a conical intersection leads to two photoproduct valleys.*

In the limit of a cold excited state reactant, one assumes that the decay will take place near the tip of the cone and with a very small excited state velocity. As discussed above, in this case one expects that the initial motion occurring after the decay will be controlled by the structure of the ground state surface. In order to understand this motion it is convenient to analyze the pattern of the ground state steepest descent lines emerging from the cone tip in the following way. We plot a series of steepest descent lines starting from *evenly* distributed points along the circle of radius *d*. The result of this exercise is shown in Figure 2. It can be seen that, because the cone is elliptic, the series of steepest descent lines rapidly separates into two distinct bundles of slightly diverging lines. The bundles of steepest descent lines admit a simple physical interpretation in terms of infinitely damped classical trajectories of a particle initially placed on the tip of the cone. Thus, when downhill motion is initiated by small random perturbations, these trajectories point preferentially toward specific regions of the

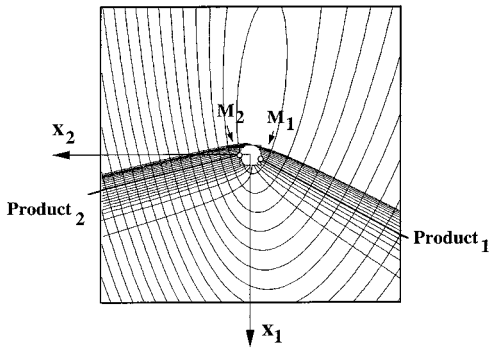

Figure 2. Contour plot of $\mathbf{E}_{gs}$ along the branching plane (x_1,x_2) showing the distribution of 36 steepest descent lines starting from equally spaced points along the circle defined in Figure 1a. The two steepest descent lines which depart from the energy minima M_1 and M_2 (see Figure 1) are also reported.

configuration space. The two IRD defined above represent unambiguously each bundle of infinitely damped classical trajectories in the vicinity of the conical intersection point. In the next section we will see that bundles of undamped trajectories generated via semiclassical dynamics simulations on a realistic potential energy surface may still be adequately represented by IRD, provided the initial kinetic energy is small.

For the elliptic (i.e. first-order[17]) cone model, discussed above, there can be at most two minima (M_1 and M_2) defining two distinct IRD (excluding the case where the cone becomes circular in which case there are an infinite number of equivalent directions of relaxation).[17] These minima are located on the branching plane (x_1,x_2). However, this model of the potential energy sheets at a conical intersection point is not general enough to give a correct description of *all* relaxation paths for a real system. Firstly, as seen in Scheme 1, there may be more than two possible IRD originating from the same conical intersection. Secondly, some IRD may lie "out" of the branching plane since the real (x_1,x_2) space is, in general, curved.[17] However, the ideas introduced above can be easily extended to search for IRD in the full *n*-dimensional space surrounding a conical intersection point by replacing the circular cross section with a (hyper)spherical cross section centered at the vertex of the cone as shown in Figure 3. Thus the search for energy minima in a one-dimensional circular cross section (i.e. the circle in Figure 1a) is merely extended to an $n - 1$ dimensional spherical cross section of the ground state potential energy surface (i.e. a hypersphere), and the IRD will then be defined by the energy minima located on the hypersphere. If the radius *d* defining the sphere is small enough, this hyperspherical cross section must contain the "starting points" for *all* relaxation paths departing from the cone vertex even if they are located far from the branching plane (x_1,x_2) as illustrated in Figure 3. Indeed, for a sufficiently small value of *d*, the relaxation path from the conical intersection will be approximately orthogonal to the sphere surface. In fact, if *d* becomes large, then the minima may still lie *close* to the true path, but not *on it* because the curvature of the path has been ignored. From a practical point of view, locating stationary points on the hypersphere is just a special case of constrained geometry optimization with one "frozen" variable *d*. Both minima and the transition structures connecting them (for instance HTS_{12} in Figure 3 connects HM_1 and HM_2) can be located. From the mechanistic point of view, the hypersphere minima define the relaxation paths (i.e. the IRD) from the cone vertex. Similarly, the transition structures on the hypersphere define the ridges (RDG) which separate pairs of different relaxation paths.

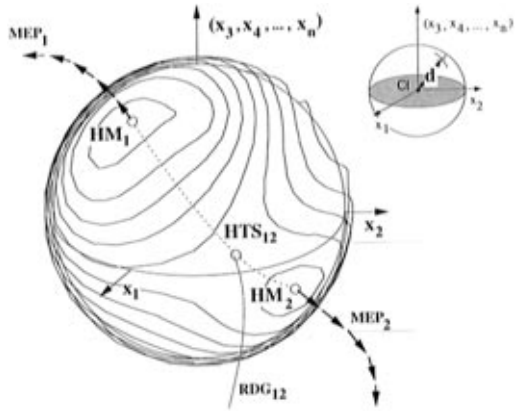

Figure 3. Spherical contour plot illustrating the behavior of $\mathbf{E}_{gs}$ along a hyperspherical cross section centered on a nonideal (i.e. nonelliptic) conical intersection point. The directions of the "ideal" tangent branching plane and tangent intersection space (see section 2) are also illustrated in the figure. Notice that the position of the hyperspherical energy minimum HM_1 lies well above the branching plane. HM_1 is connected to a second minimum HM_2 via the transition structure HTS_{12}. These minima on the hypersphere define two MEP in the full coordinate space of the system which describes the two distinct relaxation paths on the ground state potential energy sheet. Similarly HTS_{12} defines an energy ridge (RDG_{12}) which separates the two energy valleys where relaxation can occur.

We must emphasize that the procedure outlined above is designed to locate the points where the relaxation paths begin (i.e. they define the IRD). Once these points have been found for some small value of *d*, then one must compute the associated MEP which defines the relaxation paths leading to a ground state energy minimum. Thus the approach outlined above provides a systematic way to find the MEP connecting the vertex of the cone to the various ground state photoproduct wells. Since more than one MEP originates from the same conical intersection point, this procedure also describes the branching of the excited state reaction path occurring at the intersection point.

3. Computational Details

Locating stationary points on the hypersphere involves constrained geometry optimization, in mass-weighted coordinates, with a frozen variable *d*. While all results (IRD vectors and MEP coordinates) in this paper are given in mass-weighted Cartesian coordinates, the actual computations are carried out using mass-weighted internal coordinates as described in ref 18. Thus, the mass-weighted internal coordinate variables, the gradients, and the second derivatives are merely transformed to the space of the $n - 1$ independent "polar angles" (i.e. rotations) that the vector **d** (of length *d*) makes with a suitable reference axis system. One then searches for minima and transition states in this space using standard methods implemented using these polar angles as the variables. We have presented the full mathematical details elsewhere.[19] The nature of the stationary points can be tested by projecting the force constant matrix onto the hypersphere surface. Once a minimum on the hypersphere has been fully optimized, the MEP describing the associated relaxation process is determined by computing the steepest descent path in mass-weighted internal coordinates using the usual Gonzalez and Schlegel[18] IRC method (the energy gradient is chosen as the initial search direction). In a manner analogous to the MEP for thermal reactions, this steepest descent path provides a "structural" (i.e. infinitely slow motion) description of the relaxation process. All computations have been carried out using the GAUSSIAN92 package[20] at the ab initio CAS-SCF/6-31G*[21] level of theory. The choice of active space

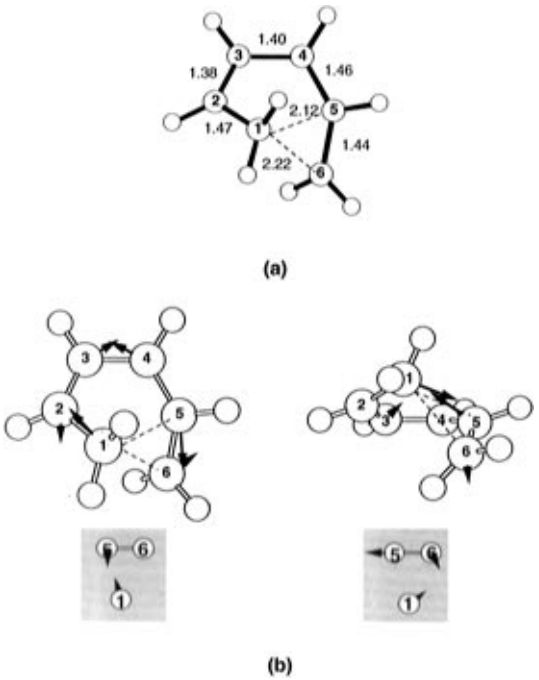

Figure 4. (a) Top view of the ab initio-optimized conical intersection structure CI_{CHD}. The relevant geometrical parameters are given in angstroms. (b) Top view (left) of the derivative coupling vector $\mathbf{x}_1$ and front view (right) of the gradient difference vector $\mathbf{x}_2$ computed at CI_{CHD}. See also ref 13. The motions of C_1, C_6, and C_5 are shown inset for comparison with Figure 9.

in our computations is unambiguous and is comprised of the four electrons and orbitals which form the π-system of CHD plus the two CH_2-CH_2 σ and σ^* electrons and orbitals (or, equivalently, the six electrons and orbitals which form the π-system of HT). The effect of the dynamic electron correlation on the relevant energy profiles and surface topology has been checked using a second-order multireference Møller−Plesset (MP2) perturbation method (CAS-PT2F),[22] and the numerical results are included as Supporting Information. The position of the conical intersection shifts slightly, and the excited state energy barrier which controls the decay decreases from 10 to ~3 kcal mol^{-1} (consistent with the 1 kcal mol^{-1} energy barrier computed in our previous work[13] using a more approximate excited state path and a different multireference MP2 method[23]). However the surface topology is unchanged.

4. "Product-Formation" Paths for the Cyclohexadiene/*cZc*-Hexatriene Photochemical Interconversion

In order to compute the product-formation paths of Scheme 1, we have applied the methodology illustrated above to the fully optimized conical intersection structure CI_{CHD} given in Figure 4a. As we will report in subsection (i), the results of these computations yield a description of the ground state relaxation paths departing in the vicinity of the decay point (as mentioned in the previous section the coordinate system used in this paper for describing the IRD vectors and MEP coordinates is mass-scaled Cartesian). The relevance of this structural (i.e. nondynamical) information for the comprehension of the mechanism of the CHD/*cZc*-HT photochemical interconversion in solution is confirmed using semiclassical dynamics. Thus in subsection (ii) we present the results of a simulation of the motion occurring in the vicinity of the conical intersection on a 36-dimensional model potential energy surface.

(i) Ground State Product-Formation Paths. The ground state potential energy surface surrounding CI_{CHD} has been scanned in different hyperspherical cross sections with radii d ranging

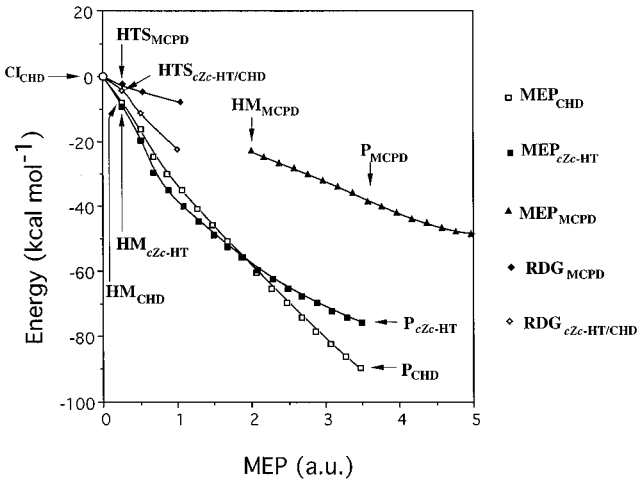

Figure 5. Ab initio CAS-SCF/6-31G* MEP (MEP_{CHD}, MEP_{cZc-HT}, and MEP_{MCPD}) and ridges ($RDG_{cZc-HT/CHD}$, RDG_{MCPD}) starting in the vicinity of the optimized conical intersection CI_{CHD}. The arrows HM_{CHD}, HM_{cZc-HT}, and HM_{MCPD} indicate the starting points of the MEP (i.e. define the corresponding IRD) located on hyperspherical cross sections with radii 0.25, 0.25, and 2.0 amu$^{1/2}$ bohr, respectively. Similarly, $HTS_{cZc-HT/CHD}$ and HTS_{MCPD} indicate the starting points of the ridges on the hyperspherical cross section with radii 0.25 amu$^{1/2}$ bohr. P_{CHD}, P_{cZc-HT}, and P_{MCPD} are selected points along the same MEP located about 3.5 amu$^{1/2}$ bohr far from CI_{CHD}.

TABLE 1: CAS-SCF/6-31G* Energies for the Optimized Conical Intersection CI_{CHD} and Hypersphere Minima (HM) and Transition Structures (HTS) Optimized in Its Vicinity

structure	energy (au)	radius d (au)	path to
CI_{CHD}	−231.720 80	0.00	
HM_{CHD}	−231.734 00	0.25	CHD
HM_{cZc-HT}	−231.735 94	0.25	*cZc*-HT
HTS_{MCPD}	−231.724 76	0.25	
$HTS_{cZc-HT/CHD}$	−231.727 65	0.25	
HM_{MCPD}	−231.756 63	2.00	MCPD
$HM_{cZc-HT*}$	−231.733 46	1.50	*cZc*-HT*

from 0.25 to 3.0 amu$^{1/2}$ bohr. For each value of the radius, the hypersphere has been searched for the presence of stationary points (e.g. energy minima and transition structures), which have been optimized using the method briefly illustrated in section 3. The results obtained with this procedure are collected in Table 1 and Figures 5, 6 and 7.

For the smallest radius (i.e. d = 0.25 amu$^{1/2}$ bohr), four stationary points (indicated as HM_{cZc-HT}, HM_{CHD}, $HTS_{cZc-HT/CHD}$, and HTS_{MCPD} in Table 1, Figures 5 and 6) have been located on the hyperspherical cross section. The points HM_{cZc-HT} and HM_{CHD} define the IRD of two different ground state relaxation paths leading to *cZc*-HT and CHD, respectively. The energy profiles along these paths are reported in Figure 5 as a function of the step along the corresponding MEP coordinate. The structures in Figure 6 show the direction of the energy gradient, in the full space of Cartesian coordinates, at these stationary points. Clearly, the gradients at HM_{cZc-HT} and HM_{CHD} are directed toward the real minima, and the conventional IRC computations beginning at the hypersphere minima use the gradients shown in Figure 6 as the initial search direction. The actual change in molecular geometry of the optimized molecular structure with respect to the vertex of the cone CI_{CHD} is very small indeed. (For points on the 0.25 amu$^{1/2}$ bohr radius hypersphere cross section, the RMS geometry change is <0.01 Å for bond lengths and <1.0° for bond angles and torsions.) Accordingly, we also indicate the direction of the relaxation process associated with each optimized minimum by plotting the structures about 3.5 amu$^{1/2}$ bohr from CI_{CHD} along the

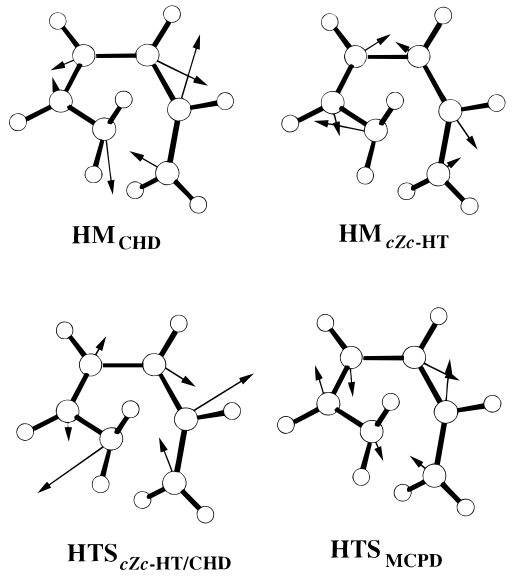

Figure 6. Structures and cartesian energy gradients (arrows) at the HM_{CHD}, HM_{cZc-HT}, $HTS_{cZc-HT/CHD}$, and HTS_{MCPD} optimized structures.

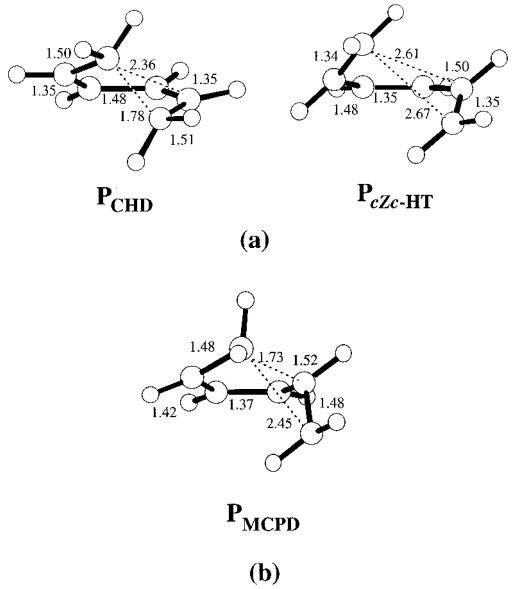

Figure 7. Relevant structural parameters of the P_{CHD}, P_{cZc-HT}, and P_{MCPD} optimized MEP structures. Bond length values in angstroms.

computed MEP. The structures P_{CHD} and P_{cZc-HT} shown in Figure 7a correspond to points located along the MEP starting at HM_{CHD} and HM_{cZc-HT}. A comparison of the geometry of these points with CI_{CHD} (see Figure 4) shows that these MEP describe the relaxation processes leading to the CHD and *cZc*-HT ground state products, respectively. The first process (starting at HM_{CHD}) involves the formation of the C_6-C_1, C_5-C_4, and C_3-C_2 bonds, the second (starting at HM_{cZc-HT}) involves the formation of the C_6-C_5, C_4-C_3, and C_2-C_1 bonds.

The transition states $HTS_{cZc-HT/CHD}$ and HTS_{MCPD} located on the 0.25 amu$^{1/2}$ bohr hypersphere connect the two energy minima HM_{cZc-HT} and HM_{CHD} on the hypersphere surface. While these structures have no direct mechanistic significance, they do enable the visualization of the topology of the hypersphere in terms of the conical intersection model shown in Figure 1a. Again, because of the small value of d these structures are not plotted. However the gradients given in Figure 6 do indicate that these structures are located on very different regions of the hypersphere. While $HTS_{cZc-HT/CHD}$ connects HM_{cZc-HT} and HM_{CHD} on one region of the sphere, HTS_{MCPD}

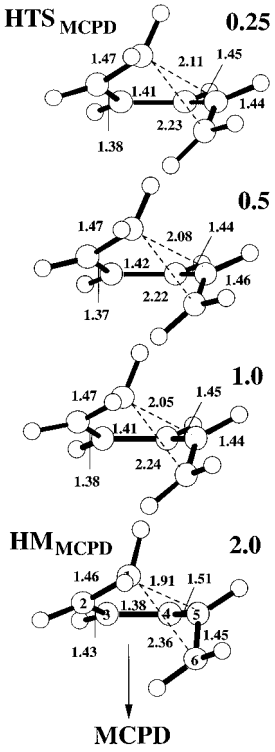

Figure 8. From top to bottom: optimized transition structures located on the hyperspheres with 0.25, 0.5, and 1.0 amu$^{1/2}$ bohr radii and defining the RDG_{MCPD} ridge. The last structure is a minimum located on the hypersphere with 2.0 amu$^{1/2}$ bohr radius and corresponds to the point where the relaxation path to MCPD (MEP_{MCPD}) "begins". The relevant geometrical parameters are given in angstroms.

connects HM_{CHD} and HM_{cZc-HT} on a different part of the cone body. As discussed in section 2, $HTS_{cZc-HT/CHD}$ and HTS_{MCPD} define two energy ridges in the full configuration space of the molecule. We have further documented these ridges by optimizing the transition structures located on three hyperspherical cross sections with increasing values of the radius (i.e. 0.25, 0.5, 1.0 amu$^{1/2}$ bohr). To summarize, the results in Figure 5 clearly show that, in the vicinity of the decay point, there are two relaxation paths (MEP_{CHD} and MEP_{cZc-HT}) with two ridges ($RDG_{cZc-HT/CHD}$ and RDG_{MCPD}) which separate them in agreement with the model conical intersection of Figure 1a.

The path leading to the third possible primary photoproduct, MCPD, cannot be located in the immediate vicinity of the conical intersection; it appears that the minimum HM_{MCPD} can be located only 2.0 amu$^{1/2}$ bohr away from the conical intersection point. However this hypersphere minimum lies in the same direction as the RDG_{MCPD} ridge. Thus, as shown in Figure 8, the structures of the hypersphere transition states found at $d = 0.25$, 0.5, and 1.0 amu$^{1/2}$ bohr and defining RDG_{MCPD} describe a change of the CI_{CHD} structure toward HM_{MCPD}. Thus, as we will discuss in the conclusion section, while HM_{MCPD} lies, basically, along the same direction of the ridge RDG_{MCPD}, this ridge is expected to split into two new ridges comprising the MCPD valley in the region near $d = 1.0$ amu$^{1/2}$ bohr. The energy profile of the MEP leading to MCPD is compared to the others in Figure 5 (MEP_{MCPD}), and the corresponding coordinate is characterized in Figure 7b through structure P_{MCPD}. Thus, the results of our computations establish that there is no relaxation path which points toward the MCPD product starting in the immediate vicinity of the tip of the cone. On the other hand, the existence of an energy minimum on the hypersphere of 2.0 amu$^{1/2}$ bohr radius indicates that such a path begins in a region slightly away from the decay point. In this region, the geometry of the system and the relaxation paths are mainly

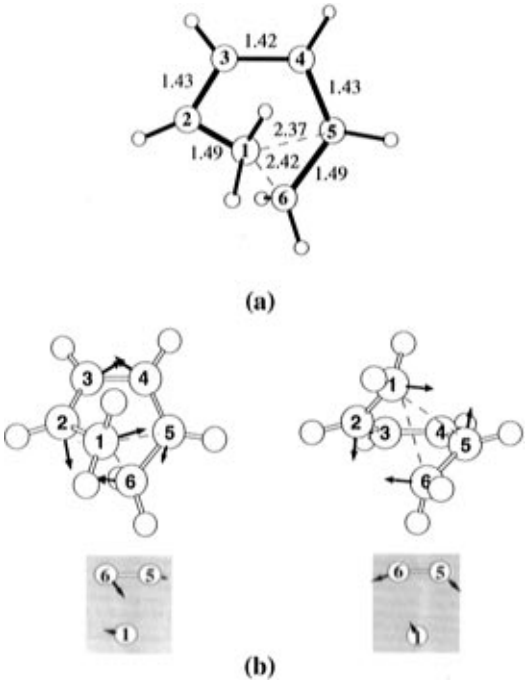

Figure 9. (a) Top view of the MM-VB-optimized conical intersection structure CI_{CHD}. The relavant geometrical parameters are given in angstroms. (b) Top view (left) of the derivative coupling vector $\mathbf{x}_1$ and front view (right) of the gradient difference vector $\mathbf{x}_2$ at CI_{CHD}. The motions of C_1,C_6, and C_5 are shown inset for comparison with Figure 4.

determined by the interaction between the singly occupied orbitals in C_1-C_5 and in C_4-C_3 which control the process of bond formation in MCPD (see Figure 8 for labels).

(ii) Semiclassical Dynamics Simulations. The IRD computations have demonstrated the existence of ground state paths (see Figure 5) leading from the vertex of the cone to the CHD and *cZc*-HT photoproduct basins. A path yielding the third photoproduct, MCPD, has also been found, but this channel begins some way from the tip of the cone. Such nondynamical information suggests that the quantum yield of the two main products would be similar and that, due to the unfavorable topology of the ground state surface, MCPD would be produced in a very low yield. To conclude this study, we investigate the decay dynamics of trajectories starting from a "circle" of points around the conical intersection, with the initial kinetic energy distributed in randomly sampled vibrational modes. These computations have been carried out using a trajectory-surface-hopping (TSH) method and a hybrid molecular mechanics valence bond (MM−VB) force field to model the ab initio potentials (details can be found elsewhere[24]). The dynamics results give further support to the idea that decay of the $2A_1$ *cZc*-HT* intermediate via CI_{CHD} results mainly in relaxation along the ground state MEP_{CHD} and MEP_{cZc-HT} paths (and that the MEP_{MCPD} path is not populated significantly).

For the dynamics simulations to be meaningful, we must provide evidence that the 36-dimensional MM-VB potential energy surface reproduces the important features of the ab initio surface in the region of the conical intersection. Firstly, the geometry of the MM-VB-optimized CI_{CHD} structure is shown in Figure 9 together with the associated $\mathbf{x}_1$ and $\mathbf{x}_2$ vectors. If one compares the vectors associated with C_1-C_5, C_5-C_6, and C_1-C_6 motion (shown in inset, Figures 9 and 4), it is apparent that the MM-VB result is in qualitative agreement with the corresponding ab initio data. Secondly, in order to demonstrate that the ab initio reaction paths exist on the MM-VB surface, we have computed a series of 20 ground state steepest descent

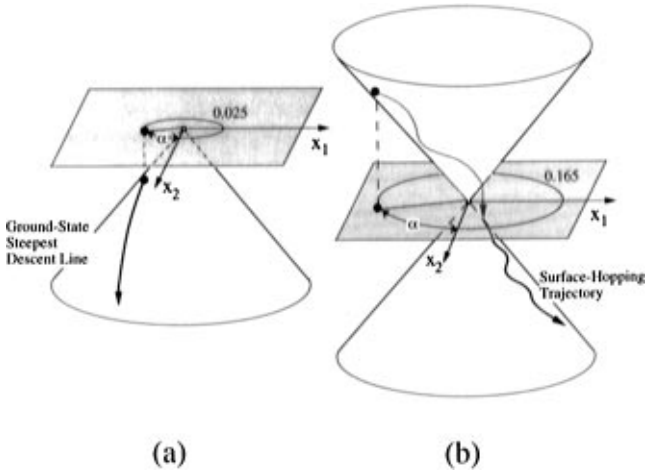

Figure 10. (a) Schematic representation of a ground state steepest descent line generated from a point on the (0.025 amu$^{1/2}$ bohr radius) circle located on the branching plane (x_1,x_2). (b) Schematic representation of a surface hopping trajectory generated from a point on the (0.165 amu$^{1/2}$ bohr radius) circle located on the branching plane (x_1,x_2).

paths in mass-weighted coordinates, starting in the vicinity of the tip of the cone (see Figure 10a). In Figures 1 and 2 we have shown that the entry channel is contained in the branching plane (x_1,x_2). Thus, for simplicity, these steepest descent paths were computed starting at points evenly distributed along a small circle (radius 0.025 amu$^{1/2}$ bohr) contained in this plane. The resulting pattern of steepest descent lines identifies the possible ground state channels leading directly from the apex of the cone. The "width" of the catchment region is given by a many-to-one correlation between the starting angles and the distinct points where the steepest descent lines terminate.

In Figure 11a we show the distribution of the starting points in terms of the values of the relevant coordinates C_5-C_1 and C_6-C_1. The C_6-C_1 distance is at its minimum near 0° on the circle and is at its maximum near 180°. The C_5-C_1 distance peaks at about 108° and has its minimum between 288° and 306°. The 20 computed steepest descent lines are labeled according to the molecular structures at the termination of points (i.e. either CHD, *cZc*-HT, or MCPD). The observed distribution of CHD and *cZc*-HT labeled lines is given in Figure 11b, and it is consistent with the pattern seen in the elliptic cone (see Figure 2 in section 2). The steepest descent lines simply go to CHD or *cZc*-HT, depending on which side of the ridge they are start. As expected, steepest descent lines leading to *cZc*-HT (i.e. ring-opening) only occur where the C_6-C_1 distance is near the maximum on Figure 11a. However, a single steepest descent line (at 306°) finds a path to the third product, MCPD, consistent with the fact that at 306° the C_1-C_5 distance is at a minimum. This is an artifact that arises from the fact that the MMVB potential surface is slightly different from the ab initio surface and the MCPD "relaxation channel" has a very small projection onto the branching space near the apex of the cone. From this simple analysis we must conclude that (with respect to the branching space, at least) there is a limited accessibility to MCPD from the apex of the cone, even for the MM-VB model surface. In conclusion, the optimized CI_{CHD} structure, branching plane, and steepest descent lines analysis suggests that the structure of the MM-VB potential energy surface is consistent with the structure of the ab initio surface with the exception of the very small projection of the MCPD channel onto the branching space.

The initial decay dynamics through the conical intersection can be studied by computing and analyzing ensembles of semiclassical trajectories. Accordingly, 20 "packets" of 64

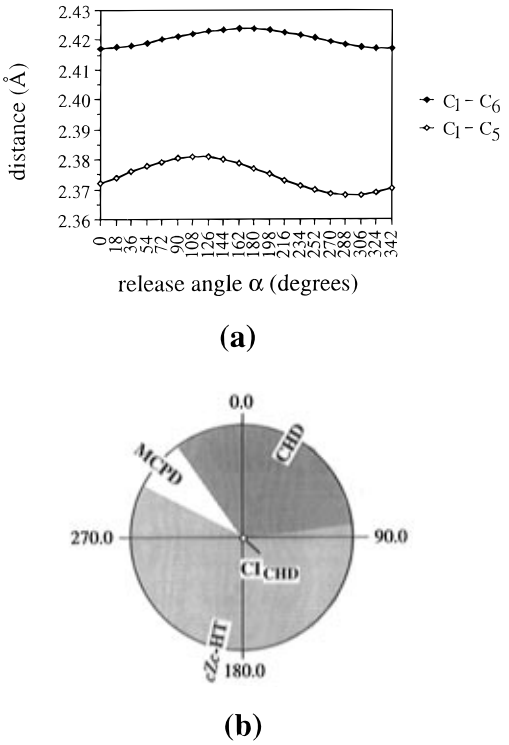

Figure 11. (a) Values of the C_6-C_1 and C_5-C_1 bond distances for the 20 points chosen on a 0.025 amu$^{1/2}$ bohr radius circle of Figure 10a. (b) Distribution of the 20 steepest descent lines released from evenly spaced points of a 0.025 amu$^{1/2}$ bohr radius branching plane circle (angle α in degrees). See also Table 3 in the supporting information.

trajectories have been generated, starting from excited state points located around a circle in the branching plane as illustrated in Figure 10b. The radius of the circle (0.165 amu$^{1/2}$ bohr) and the initial conditions have been chosen in order to produce a total excited state excess vibrational energy compatible with the average energy available at room temperature (i.e. ∼20 kcal mol^{-1}). A radius was chosen which typically raises the potential energy by 15 kcal mol^{-1} above the apex of the cone. At each point on this circle we randomly sample the vibrational modes of the molecule to generate the initial conditions for the ensemble. This vibrational sampling has a range of 2−3 kcal mol^{-1} to avoid the packets overlapping.

In general, the dynamics results obtained agree well with the qualitative predictions obtained from the study of the relaxation MEP of Figure 5. Since the trajectories are starting close to the intersection, they spend a very short time on the excited state surface before hopping to the ground state on the first oscillation (in most cases). Hence, the subsequent paths taken will depend almost entirely on the ground state topology and the angle at which the trajectories pass through the intersection. For each angle, the 64 trajectories of the packet are labeled in the same way as the steepest descent lines of Figure 11 (i.e. according to the molecular structures of the product). Figure 12 shows the percent yields obtained as a function of the initial angle in the branching space.[25] Clearly, the CHD and *cZc*-HT photoproducts predominate, and we see a simple distribution as the angle changes. This is consistent with there being two ridges (at about 90 and 270°) funneling the trajectories to each photoproduct. However, at a small range of angles (near 90°), the trajectories populate a channel leading to the MCPD product. This is expected from the artifact seen in steepest descent lines computed with the MM−VB surface (Figure 11b), where we see the narrow MCPD relaxation channel at 306°.

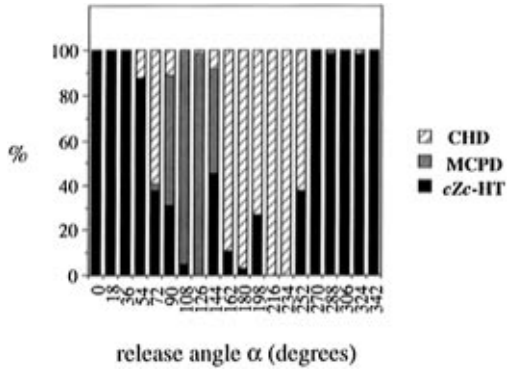

Figure 12. Percent yield for each packet of 64 hopping trajectories released from the branching space circle of Figure 10b.

SCHEME 3

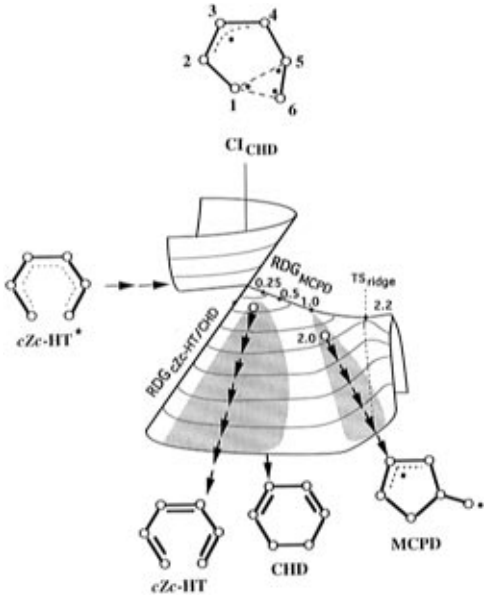

5. Conclusions

In this paper, we have presented a computationally effective definition of the initial relaxation directions from the tip of a conical intersection. The MEP generated from each IRD provides a natural continuation of the excited state MEP connecting the photoexcited reactant to the conical intersection. Accordingly, the IRD can be used to perform a systematic investigation of the product-formation paths in organic (and inorganic) photochemistry where a conical intersection provides the decay channel to the ground state and where full dynamics treatments are not feasible. We stress that the nondynamical information provided by the IRD can be used to provide insight into the photochemical mechanism of relatively cold excited state species where slow motion and/or thermal equilibration is possible (achieved in cool jet, in matrices, and in solution). Under such conditions we show that the same conclusions can be drawn from a search for IRD and from semiclassical trajectories.

In the hypothesis that significant picosecond vibrational relaxation takes place in solution at room temperature, the IRD computed in the region of the conical intersection provide insight into the mechanism of the CHD/*cZc*-HT photochemical interconversion. According to our results, the key structural features controlling the product-formation process resulting from the decay of the $2A_1$ excited state intermediate *cZc*-HT* are illustrated in Scheme 3.

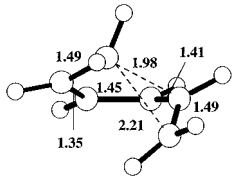

Figure 13. Relevant structural parameters of the fully optimized unconstrained transition structure TS_{ridge}. Bond length values in angstroms.

In this scheme, white areas represent energy ridges and shaded areas represent energy valleys (see also point (ii) in the Supporting Information). The *cZc*-HT* intermediate, which is produced by either CHD or *cZc*-HT irradiation, decays via a facile vibrational displacement, leading toward the CI_{CHD} decay point located 1−3 kcal mol^{-1} higher in energy. After decay, the reaction path bifurcates along two ground state relaxation coordinates MEP_{CHD} and MEP_{cZc-HT} (full arrows in Scheme 3) whose energy profiles are reported in Figure 5. A third relaxation coordinate, MEP_{MCPD}, is not directly connected to the conical intersection point CI_{CHD} and originates after the energy ridge RDG_{MCPD} splits into two new ridges (comprising the MCPD valley) around 1.0 amu$^{1/2}$ bohr distance from the decay point. This view is also supported by the following additional result: a high energy, unconstrained transition structure (i.e. a transition structure in the full *n*-dimensional space) has been optimized in the vicinity of the RDG_{MCPD} ridge (see TS_{ridge} in Scheme 3 and Figure 13). A conventional MEP computation starting at TS_{ridge} which is located 0.1 kcal mol^{-1} below HM_{MCPD} and has a transition vector tangent to the 2.2 amu$^{1/2}$ bohr hypersphere shows that this structure connects the MCPD and CHD valleys (see dashed line in Scheme 3). Thus the existence of TS_{ridge} indicates that at $d \sim 2.0$ amu$^{1/2}$ bohr the original RDG_{MCPD} ridge (which separates the *cZc*-HT and CHD valleys) has split so that the MCPD valley is comprised between two ridges which separate the CHD and MCPD valleys, and the MCPD and *cZc*-HT valleys respectively. While we have demonstrated that TS_{ridge} is located on the first ridge, we have not been able to computationally characterize the second ridge.

The distance of the hyperspherical minima (HM_{CHD}, HM_{cZc-HT}, and HM_{MCPD}) from the decay point and the magnitude of the slope of the associated MEP provide qualitative information on the extent of the "catchment region" associated with a specific photoproduct (see shaded regions in Scheme 3). A MEP which develops close to the conical intersection point and which is lower in energy will be associated with a larger "catchment region", and therefore there will be a higher probability of populating the associated MEP upon decay from the conical intersection. Both Figure 5 and the dynamics results in Figure 12 suggest that the size of the CHD and *cZc*-HT catchment regions must be similar. In fact, both the energy profiles (MEP_{CHD} and MEP_{cZc-HT} in Figure 5) and the percent yields produced via semiclassical dynamics simulations (i.e. the CHD and *cZc*-HT yields in Figure 12) are similar for these two paths. Thus we expect that the decay of *cZc*-HT* will generate the products CHD and *cZc*-HT with similar yields. Hence, the photolysis of CHD is predicted to generate *cZc*-HT with a quantum yield $\Phi_{cZc-HT} < 1$ because of the competitive CHD back-formation. On the other hand, our computational results suggest that MCPD can only be a very low quantum yield primary photoproduct in the photolysis of CHD. The MCPD product formation path has a higher MEP energy profile with respect to the other paths. Further, the MCPD product formation path is topologically inhibited since, in the immediate vicinity of the conical intersection, it corresponds to a ridge (i.e. RDG_{MCPD}), and ridge-like paths will be only populated at very large kinetic energies. For this reason, the photolysis of either CHD or *cZc*-HT must have a similar outcome. In fact, since both these reactants yield the same *cZc*-HT* $2A_1$ intermediate (see discussion in ref 13), *cZc*-HT is predicted to yield CHD with a quantum yield $\Phi_{cZc-HT\rightarrow CHD}$ which is related to the quantum yield of *cZc*-HT produced via CHD photolysis ($\Phi_{CHD\rightarrow cZc-HT}$) by the relation $\Phi_{cZc-HT\rightarrow CHD} \approx (1 - \Phi_{CHD\rightarrow cZc-HT})$.

The interpretation of the CHD/*cZc*-HT photolysis just presented is compatible with the available experimental data. The 1−3 kcal mol^{-1} excited state energy barrier computed via multireference MP2 theory is consistent with the observed 6 picosecond lifetime of the $2A_1$ state following CHD direct irradiation.[9] While there are no measurements of $\Phi_{CHD\rightarrow CHD}$ (i.e. CHD back-formation during photolysis of CHD) or $\Phi_{cZc-HT\rightarrow CHD}$ (i.e. CHD formation during photolysis of *cZc*-HT), $\Phi_{CHD\rightarrow cZc-HT}$ is 0.41[9], i.e. suggesting efficient CHD back-formation. On the other hand, irradiation of 2,5-di-*tert*-butylhexa-1,3,5-triene produces 1,4-di-*tert*-butylcyclohexa-1,3-diene with a 0.54 quantum yield. The reverse reaction occurs with a 0.46 quantum yield[16] in agreement with the predicted relationship $\Phi_{CHD\rightarrow cZc-HT} \approx (1 - \Phi_{cZc-HT\rightarrow CHD})$. In other substituted and polycyclic molecules,[26] steric and strain effects may greatly differentiate the slopes of the MEP_{CHD} and MEP_{cZc-HT} energy profiles, leading to values of Φ_{CHD} and Φ_{cZc-HT} far from 0.5. However, the relationship given above appears to hold even in these cases.[13]

Acknowledgment. This research has been supported in part by the EPSRC (U.K.) Grants GR/J25123 and GR/K04811 and in part by CINECA (Italy). Dynamics computations were performed on Cray-T3d machines at Cineca and Edinburgh Parallel Computing Center (EPCC). We are also grateful to NATO for a travel grant (CRG 950748).

Supporting Information Available: (i) An appendix, one scheme (Scheme 4), and one figure (Figure 14) on the relationship between the excited state reaction and the ground state relaxation paths in the CHD/*cZc*-HT photochemical interconversion, (ii) an appendix, one figure (Figure 15), and one table (Table 3) on the multireference second-order MP2 computation of the energetics of the excited and ground state paths, and (iii) one table (Table 2) giving the numerical results associated with Figure 11b (7 pages). Ordering information is given on any current masthead page.

References and Notes

(1) Klessinger, M. *Angew. Chem., Int. Ed. Engl.* **1995**, *34*, 549−551.

(2) Michl, J.; Bonacic-Koutecky, V. *Electronic Aspects of Organic Photochemistry*; Wiley: New York, 1990.

(3) For recent results see: (a) Celani, P.; Bernardi, F.; Olivucci, M.; Robb, M. A. *J. Chem. Phys.* **1995**, *102*, 5733. (b) Heumann, B.; Schinke, R. *J. Chem. Phys.* **1994**, *101*, 7488−7499. (c) Yarkony, D. R. *J. Chem. Phys.* **1994**, *100*, 3639. (d) Mielke, S. L.; Tawa, G. J.; Truhlar, D. G.; Schwenke D. W. *J. Am. Chem. Soc.* **1993**, *115*, 6436. (e) Muller, H. *et al. Chem. Phys. Lett.* **1992**, *197*, 599. (f) Woywod, C.; Domcke, W.; Sobolewski, A. L.; Werner H-J. *J. Chem. Phys.* **1994**, *100*, 1400. (g) Atchity, G. J.; Xantheas, S. S.; Elbert, S. T.; Ruedenberg, K. *J. Chem. Phys.* **1991**, *94*, 8054.

(4) (a) Petek, H.; Bell, A. J.; Christensen, R. L.; Yoshiara, K. *SPIE*, **1992**, *1638*, 345−356. (b) Petek, H.; Bell, A. J.; Choi, Y. S.; Yoshiara, K.; Tounge, B. A.; Christensen, R. L. *J. Chem. Phys.* **1993**, *98*, 3777−3794.

(5) Celani, P.; Garavelli, M.; Ottani, S.; Bernardi, F.; Robb, M. A.; Olivucci, M. *J. Am. Chem. Soc.* **1995**, *117*, 11584−11585.

(6) Semiclassically, the probability of radiationless decay via the Landau−Zener model as shown by Desouter-Lecomte and Lorquet (Desouter-Lecomte, M.; Lorquet, J. C. *J. Chem. Phys.* **1979**, *71*, 4391, 3661) is given as

$$P = \exp[-(\pi/4)\xi]$$

where ξ is the Massey parameter given as

$$\xi = \frac{\Delta E(\mathbf{q})}{\frac{h}{2\pi}|\dot{q}|g(q)|}$$

where **q** is a vector of nuclear displacement coordinates. The term $g(q)$ is the nonadiabatic coupling matrix element defined as

$$g(q) = \langle \psi_1 | \partial \psi_2 | \partial \mathrm{q} \rangle$$

while $|\dot{q}|$ is the magnitude of the velocity along the reaction path **q** and ΔE is the energy gap between the two states ψ_1 and ψ_2. Unless ΔE is less than about 2 kcal mol^{-1}, the decay probability is vanishing small. However, as we approach a point where the surfaces cross, the decay probability becomes unity.

(7) (a) Rejto, P. A.; Bindewald, E.; Chandler, D. *Nature* **1995**, *375*, 129−131. (b) Liu, Q.; Wang, J.-K.; Zewail, A. H. *J. Phys. Chem.* **1995**, *99*, 11321.

(8) (a) Jimenez, R.; Fleming, G. R.; Kumar, P. V.; Maroncelli, M. *Nature* **1994**, *369*, 471−473. (b) Liu, Q.; Wang, J.-K.; Zewail, A. H. *J. Phys. Chem.* **1995**, *99*, 11309. (c) Heikal, A. A.; Chong, S. H.; Baskin, J. S.; Zewail, A. H. *Chem. Phys. Lett.* **1995**, *242*, 380−389. (d) Zhong, Q.; Wang, Z.; Sun, Y.; Zhu, Q.; Kong, F. *Chem. Phys. Lett.* **1996**, *248*, 277−282.

(9) Reid, P. J.; Doig, S. J.; Wickham, S. D.; Mathies, R. A. *J. Am. Chem. Soc.* **1993**, *115*, 4754. However, recent experiments by Sension and co-workers (Pullen, S.; Walker, L. A., II; Donovan, B.; Sension, R. J. *Chem. Phys. Lett.* **1995**, *242*, 415−420) have indicated a $2A_1$ lifetime of ∼1 ps.

(10) (a) Koppel, H.; Domcke, W.; Cederbaum, L. S. *Adv. Chem. Phys.* **1984**, *57*, 59. (b) Manthe, U.; Koppel, H. *J. Chem. Phys*, **1990**, *93*, 1658.

(11) Truhlar, D. G.; Steckler, R.; Gordon, M. S. *Chem. Rev.* **1987**, *87*, 217. Truhlar, D. G.; Gordon M. S. *Science* **1990**, *249*, 491.

(12) McKee, M. L.; Page M. in *Reviews in Computational Chemistry*; Lipkowiz, K. B., Boyd, D. B., Eds.; VCH: New York, 1993; 4, pp 35−65.

(13) Celani, P.; Ottani, S.; Olivucci, M.; Bernardi, F.; Robb, M. A. *J. Am. Chem. Soc.* **1994**, *116*, 10141−10151.

(14) Heller, H. G.; Elliot, C. C.; Koh, K.; Al-Shihry, S.; Whittall, J. In *Photochemistry and Polymeric Systems*; Eds. Kelly, J. M., Mc Ardle, C. B., de F. Maunder, M. J., Eds.; The Royal Society of Chemistry: London, 1993; pp 156−168.

(15) (a) Jacobs, H. J. C.; Havinga, E. Photochemistry of Vitamin D and Its Isomers and of Simple Trienes. In *Advances in Photochemistry*; Pitts, J. N., Jr.; Hammond, G. S.; Gollnick, K. Eds; John Wiley & Sons: New York, 1979; Vol. 11, pp 305−373. (b) Dauben, W. G.; McInnis, E. L.; Mincho, D. M.; Photochemical Rearrangements in Trienes. In *Rearrangements in Ground and Excited States*; De Mayo, P., Ed.; Academic Press: London, 1980; Vol. 3, pp 91−129.

(16) (a) Jacobs, H. J. C. *Pure Appl. Chem.* **1995**, *67*, 63−70. (b) Brouwer, A. M.; Cornelisse, J. and Jacobs, H. J. C. *J. Photochem. Photobiol A: Chem.* **1988**, *42*, 117. (c) Brouwer, A. M.; Cornelisse, J.; Jacobs, H. J. C. *J. Photochem. Photobiol., A.* **1988**, *42*, 313.

(17) Atchity, G. J.; Xantheas, S. S.; Ruedenberg, K. *J. Chem. Phys.*, **1991**, *95*, 1862−1876.

(18) Gonzalez, C.; Schlegel, H. B. *J. Phys. Chem.* **1990**, *94*, 5523−5527.

(19) Celani, P.; Robb, M. A.; Garavelli, M.; Bernardi, F.; Olivucci, M. *Chem. Phys. Lett.* **1995**, *243*, 1−8.

(20) Frisch, M. J.; Trucks, G. W.; Head-Gordon, M.; Gill, P. M. W.; Wong, M. W.; Foresman, J. B.; Johnson, B. G.; Schlegel, H. B.; Robb, M. A.; Replogle, E. S.; Gomperts, R.; Andres, J. L.; Raghavachari, K.; Binkley, J. S.; Gonzalez, C.; Martin, R. L.; Fox, D. J.; Defrees, D. J.; Baker, J.; Stewart, J. J. P.; Pople, J. A. *Gaussian 92*, Revision B; Gaussian, Inc.: Pittsburgh, PA, 1992.

(21) Roos, B. O. *Adv. Chem. Phys.* **1987**, *69*, 399−446.

(22) Andersson, K.; Malmqvist, P.-A.; Ross, B. O. *J. Chem. Phys.* **1992**, *96*, 1218. The CAS-PT2F method is implemented in *MOLCAS*, Version 2. Andersson, K.; Blomberg, M. R. A.; Fülscher, M.; Kellö, V.; Lindh, R.; Malmqvist, P.-A.; Noga, J.; Olsen, J.; Roos, B. O.; Sadlej, A. J.; Siegbahn, P. E. M.; Urban, M.; Widmark, P. O. *MOLCAS*, Version 2; University of Lund: Lund, Sweden, 1991.

(23) (a) McDouall, J. J. W.; Peasley, K.; Robb, M. A. *Chem. Phys. Lett.* **1988**, *148*, 183. (b) Bernardi, F.; Bottoni, A.; Celani, P.; Olivucci, M.; Robb, M. A.; Venturini, A. *Chem. Phys. Lett.* **1992**, *192*, 229−235.

(24) Smith, B. R.; Bearpark, M. J.; Robb, M. A.; Bernardi, F.; Olivucci, M. *Chem. Phys. Lett.* **1995**, *242*, 27−32.

(25) The interpretation of the trajectories requires some caution. An excited state trajectory released at a branching plane angle, say "α°, can be expected to access the ground state in the region near "α + 180"° (see Figure 10b). For instance, the small number of trajectories entering the MCPD channel start near 126°, while the MEP leading to MCPD was found at an angle of 306° (i.e. ∼126 + 180). Although, of course, the trajectories are moving in all degrees of freedom, this simple interpretation in terms of angles in the branching space seems successful (presumably because most of the initial motion is in the branching space). Similarly, large yields of CHD correspond to finding MEP to CHD on the "opposite" side of the circle. Due to the very small projection of the MCPD channel into the branching space (see subsection (ii)), trajectories decaying near the apex of the cone are unlikely to populate this channel.

(26) (a) Matuszewski, B.; Burgstahler, A. W.; Givens, R. S. *J. Am. Chem. Soc.* **1982**, *104*, 6875. (b) Dauben, W. G.; Rabinowitz, J.; Vietmeyer, N. D.; Wendschuh, P. H. *J. Am. Chem. Soc.* **1972**, *94*, 4285.